

Threshold Resummation for Slepton-Pair Production at Hadron Colliders

Giuseppe Bozzi

Institut für Theoretische Physik, Universität Karlsruhe, Postfach 6980, D-76128 Karlsruhe, Germany

Benjamin Fuks and Michael Klasen*

Laboratoire de Physique Subatomique et de Cosmologie,

Université Joseph Fourier/CNRS-IN2P3, 53 Avenue des Martyrs, F-38026 Grenoble, France

(Dated: October 9, 2018)

We present a first and extensive study of threshold resummation effects for supersymmetric (SUSY) particle production at hadron colliders, focusing on Drell-Yan like slepton-pair and slepton-sneutrino associated production. After confirming the known next-to-leading order (NLO) QCD corrections and generalizing the NLO SUSY-QCD corrections to the case of mixing squarks in the virtual loop contributions, we employ the usual Mellin N -space resummation formalism with the minimal prescription for the inverse Mellin-transform and improve it by resumming $1/N$ -suppressed and a class of N -independent universal contributions. Numerically, our results increase the theoretical cross sections by 5 to 15% with respect to the NLO predictions and stabilize them by reducing the scale dependence from up to 20% at NLO to less than 10% with threshold resummation.

I. INTRODUCTION

The Minimal Supersymmetric Standard Model (MSSM) [1, 2] is one of the most promising extensions of the Standard Model (SM) of particle physics. It postulates a symmetry between fermionic and bosonic degrees of freedom in nature, predicting thus the existence of a fermionic (bosonic) supersymmetric (SUSY) partner for each bosonic (fermionic) SM particle. Its main advantages are the stabilization of the gap between the Planck and the electroweak scale [3], gauge coupling unification at high energy scales [4], and a stable lightest supersymmetric particle as a dark matter candidate [5]. Spin partners of the SM particles have not yet been observed, and in order to remain a viable solution to the hierarchy problem, SUSY must be broken at low energy via soft mass terms in the Lagrangian. As a consequence, the SUSY particles must be massive in comparison to their SM counterparts, and the Tevatron and the LHC will perform a conclusive search covering a wide range of masses up to the TeV scale.

Scalar leptons are among the lightest supersymmetric particles in many SUSY-breaking scenarios [6] and often decay into the corresponding Standard Model (SM) partner and the lightest stable SUSY particle. A possible signal for slepton-pair production at hadron colliders would thus consist in a highly energetic lepton pair and associated missing energy. An accurate calculation of the transverse-momentum spectrum [7] allows us to use the Cambridge (s)transverse mass to measure the slepton masses [8] and spin [9] and to distinguish this signal from the SM background, which is mainly due to WW and $t\bar{t}$ production [10, 11]. Current experimental (lower) limits on electron, muon, and tau slepton masses are 73 GeV, 94 GeV, and 81.9 GeV, respectively [12]. The leading-order (LO) cross section for the production of non-mixing slepton-pairs has been calculated in [13, 14, 15, 16], while the mixing between the interaction eigenstates was included in [17]. The next-to-leading order (NLO) QCD corrections have been calculated in [18], and the full SUSY-QCD corrections have been added in [19]. However, the presence of massive non-mixing squarks and gluinos in the loops makes the genuine SUSY corrections considerably smaller than the standard QCD ones.

In this paper, we extend this last work by including mixing effects relevant for the squarks appearing in the loops, and we consider the threshold-enhanced contributions, due to soft-gluon emission from the initial state. These contributions arise when the initial partons have just enough energy to produce the slepton pair in the final state. In this case, the mismatch between virtual corrections and phase-space suppressed real-gluon emission leads to the appearance of large logarithmic terms $\alpha_s^n [\ln^{2n-1}(1-z)/(1-z)]_+$ at the n^{th} order of perturbation theory, where $z = M^2/s$, M is the slepton-pair invariant mass, and s is the partonic center-of-mass energy. When s is close to M^2 , the large logarithms have to be resummed, i.e. taken into account to all orders in α_s . The convolution of the partonic cross section with the steeply falling parton distributions enhances the threshold contributions even if the hadronic threshold is far from being reached, i.e. $\tau = M^2/S \ll 1$, where S is the hadronic center-of-mass energy. Large corrections are thus expected for the Drell-Yan production of a slepton pair with invariant mass M of a few 100 GeV at the Tevatron and LHC.

*klasen@lpsc.in2p3.fr

All-order resummation is achieved through the exponentiation of the soft-gluon radiation, which does not take place in z -space directly, but in Mellin N -space, where N is the Mellin-variable conjugate to z and the threshold region $z \rightarrow 1$ corresponds to the limit $N \rightarrow \infty$. Thus, a final inverse Mellin-transform is needed in order to obtain a resummed cross section in z -space. Threshold resummation for the Drell-Yan process was first performed in [20, 21] at the leading-logarithmic (LL) and next-to-leading-logarithmic (NLL) levels, corresponding to terms of the form $\alpha_s^n \ln^{2n} N$ and $\alpha_s^n \ln^{2n-1} N$. The extension to the NNLL level ($\alpha_s^n \ln^{2n-2} N$ terms) has been carried out both for the Drell-Yan process [22] and for Higgs-boson production [23]. Very recently, even the NNNLL contributions ($\alpha_s^n \ln^{2n-3} N$ terms) became available [24, 25, 26].

In this paper, we will perform resummation for slepton-pair production at the NLL level, the reason being that away from the threshold region, the resummed calculation has to be matched to the fixed-order calculation, which is at present only known to NLO accuracy. Our analytical results for neutral (γ, Z^0) and charged (W^\pm) current slepton-pair and slepton-sneutrino associated production at NLO will be presented in Sec. II. In Sec. III, our fixed-order results will be used to perform the threshold-resummation to NLL accuracy, and numerical predictions will be made in Sec. IV. We summarize our results in Sec. V. The mixing of sfermion interaction eigenstates is discussed in App. A, and the NLO SUSY-QCD form factors for mixing squark loop contributions are collected in App. B.

II. SLEPTON-PAIR PRODUCTION AT FIXED ORDER IN PERTURBATIVE QCD

In this section, we present the leading and next-to-leading order contributions in the strong coupling constant α_s to the mass-spectrum for slepton-pair and slepton-sneutrino associated production in hadronic collisions through neutral- and charged-current Drell-Yan type processes,

$$h_a(p_a) h_b(p_b) \rightarrow \tilde{l}_i(p_1) \tilde{l}_j^{(*)}(p_2). \quad (1)$$

We define the square of the weak coupling constant $g_W^2 = e^2/\sin^2 \theta_W$ in terms of the electromagnetic fine structure constant $\alpha = e^2/(4\pi)$ and the squared sine of the electroweak mixing angle $x_W = \sin^2 \theta_W$. The coupling strengths of left- and right-handed (s)fermions to the neutral and charged electroweak currents are then given by

$$\{L_{Zff}, R_{Zff}\} = 2T_f^3 - 2e_f x_W, \quad (2)$$

$$\{L_{Z\tilde{f}_i\tilde{f}_j}, R_{Z\tilde{f}_i\tilde{f}_j}\} = \{L_{Zff} S_{i1}^{\tilde{f}} S_{j1}^{\tilde{f}*}, R_{Zff} S_{i2}^{\tilde{f}} S_{j2}^{\tilde{f}*}\}, \quad (3)$$

$$L_{Wff'} = \sqrt{2} \cos \theta_W V_{ff'}, \quad (4)$$

$$L_{W\tilde{f}_i\tilde{f}'_j} = L_{Wff'} S_{i1}^{\tilde{f}} S_{j1}^{\tilde{f}'*}, \quad (5)$$

where the weak isospin quantum numbers are $T_f^3 = \pm 1/2$ for left-handed and $T_f^3 = 0$ for right-handed (s)fermions, their fractional electromagnetic charges are denoted by e_f , and $V_{ff'}$ are the usual CKM-matrix elements. In general SUSY-breaking models, the sfermion interaction eigenstates are not identical to the respective mass eigenstates, and mixing effects must be included in the coupling strengths through the unitary matrices $S^{\tilde{f}}$ diagonalizing the sfermion mass matrices (see App. A). For purely left-handed sneutrino eigenstates $\tilde{\nu}_L$ a diagonalizing matrix is not needed, i.e. $S_{L1}^{\tilde{\nu}}=1$ and $S_{ij}^{\tilde{\nu}}=0$ otherwise. In non-minimal flavour violating (NMFV) models with inter-generational mixing, the squark and slepton (sneutrino) mass matrices become in principle six- (three-) dimensional, although flavour-changing neutral lepton currents are experimentally strongly constrained [27].

Thanks to the QCD factorization theorem, the unpolarized hadronic cross section

$$\sigma = \sum_{a,b} \int_{\tau}^1 dx_a \int_{\tau/x_a}^1 dx_b f_{a/h_a}(x_a, \mu_F^2) f_{b/h_b}(x_b, \mu_F^2) \hat{\sigma}_{ab} \left(z, M^2; \alpha_s(\mu_R^2), \frac{M^2}{\mu_F^2}, \frac{M^2}{\mu_R^2} \right) \quad (6)$$

can be written as the convolution of the relevant partonic cross section $\hat{\sigma}_{ab}$ with the universal distribution functions $f_{a,b/h_{a,b}}$ of partons a, b inside the hadrons $h_{a,b}$, which depend on the longitudinal momentum fractions of the two partons $x_{a,b}$ and on the unphysical factorization scale μ_F . The partonic scattering cross section will be expressed in terms of the SUSY particle masses $m_{\tilde{l}_i}, m_{\tilde{\nu}}, m_{\tilde{q}_i}, m_{\tilde{g}}$ and the masses of the neutral and charged electroweak gauge bosons m_Z and m_W . The dependence on the strong coupling constant α_s , the factorization and renormalization scales μ_F and μ_R , the invariant mass of the slepton pair M and the scaling variable $z = M^2/s$, where $s = x_a x_b S$ and $S = (p_a + p_b)^2$, will be explicitly shown. In QCD perturbation theory, the partonic cross section can be expanded in powers of α_s ,

$$\hat{\sigma}_{ab} \left(z, M^2; \alpha_s(\mu_R^2), \frac{M^2}{\mu_F^2}, \frac{M^2}{\mu_R^2} \right) = \sum_{n=0}^{\infty} \left(\frac{\alpha_s(\mu_R^2)}{\pi} \right)^n \sigma_{ab}^{(n)} \left(z, M^2; \frac{M^2}{\mu_F^2}, \frac{M^2}{\mu_R^2} \right). \quad (7)$$

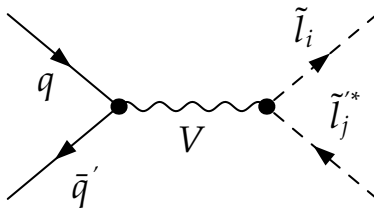


FIG. 1: Feynman diagram for slepton-pair ($V = \gamma, Z^0$) and slepton-sneutrino associated ($V = W^\mp$) production at leading order in perturbative QCD.

In this work we have computed the LO ($n = 0$) and NLO ($n = 1$) coefficients in the case of general mixing between the sfermion interaction eigenstates.

A. Total Cross Sections at Leading Order

At leading order in perturbative QCD, slepton-pair and associated slepton-sneutrino production proceed through an s -channel exchange of a photon, a Z^0 - or a W^\mp -boson,

$$\begin{aligned} q\bar{q} &\rightarrow \gamma, Z^0 \rightarrow \tilde{l}_i \tilde{l}_j^*, \\ q\bar{q}' &\rightarrow W^\mp \rightarrow \tilde{l}_i \tilde{\nu}_l^*, \tilde{l}_i^* \tilde{\nu}_l, \end{aligned} \quad (8)$$

as shown in Fig. 1. The corresponding cross sections were first calculated in [13, 14, 15, 16], and mixing effects between the interaction eigenstates relevant for third-generation sleptons were added in [17].

For neutral currents, the first coefficient of Eq. (7) is given by

$$\begin{aligned} \sigma_{q\bar{q}}^{(0)} \left(z, M^2; \frac{M^2}{\mu_F^2}, \frac{M^2}{\mu_R^2} \right) &= \sigma_0(M^2) \delta(1-z) \\ &= \frac{\alpha^2 \pi \beta^3}{9 M^2} \left[e_q^2 e_l^2 \delta_{ij} + \frac{e_q e_l \delta_{ij} (L_{Zqq} + R_{Zqq}) \operatorname{Re} [L_{Z\tilde{l}_i \tilde{l}_j} + R_{Z\tilde{l}_i \tilde{l}_j}]}{4 x_W (1-x_W) (1-m_Z^2/M^2)} \right. \\ &\quad \left. + \frac{(L_{Zqq}^2 + R_{Zqq}^2) |L_{Z\tilde{l}_i \tilde{l}_j} + R_{Z\tilde{l}_i \tilde{l}_j}|^2}{32 x_W^2 (1-x_W)^2 (1-m_Z^2/M^2)^2} \right] \delta(1-z). \end{aligned} \quad (9)$$

The three terms in Eq. (9) represent the squared photon-contribution, the photon- Z^0 interference and the squared Z^0 -contribution, respectively. The slepton-mass dependence is factorized in the velocity

$$\beta = \sqrt{1 + m_i^4/M^4 + m_j^4/M^4 - 2(m_i^2/M^2 + m_j^2/M^2 + m_i^2 m_j^2/M^4)}. \quad (10)$$

The purely left-handed charged-current cross section is easily derived from Eq. (9) by setting

$$m_Z \rightarrow m_W, \quad e_q = e_l = R_{Zqq} = R_{Z\tilde{l}_i \tilde{l}_j} = 0, \quad L_{Zqq} \rightarrow L_{Wqq'}, \quad \text{and} \quad L_{Z\tilde{l}_i \tilde{l}_j} \rightarrow L_{W\tilde{f}_i \tilde{f}_j'}, \quad (11)$$

which gives

$$\begin{aligned} \sigma_{q\bar{q}'}^{(0)} \left(z, M^2; \frac{M^2}{\mu_F^2}, \frac{M^2}{\mu_R^2} \right) &= \sigma'_0(M^2) \delta(1-z) \\ &= \frac{\alpha^2 \pi \beta^3}{9 M^2} \left[\frac{|L_{Wqq'} L_{W\tilde{l}_i \tilde{\nu}_l}|^2}{32 x_W^2 (1-x_W)^2 (1-m_W^2/M^2)^2} \right] \delta(1-z). \end{aligned} \quad (12)$$

After integration of the differential cross sections presented in [16, 17], we find agreement with the neutral-current result of [13] and the charged-current result of [16] in the limit of non-mixing mass-degenerate sleptons, obtained by setting all mixing matrices to the identity and by summing over the left- and right-handed eigenstates, as well as with the general charged- and neutral-current results of [17].

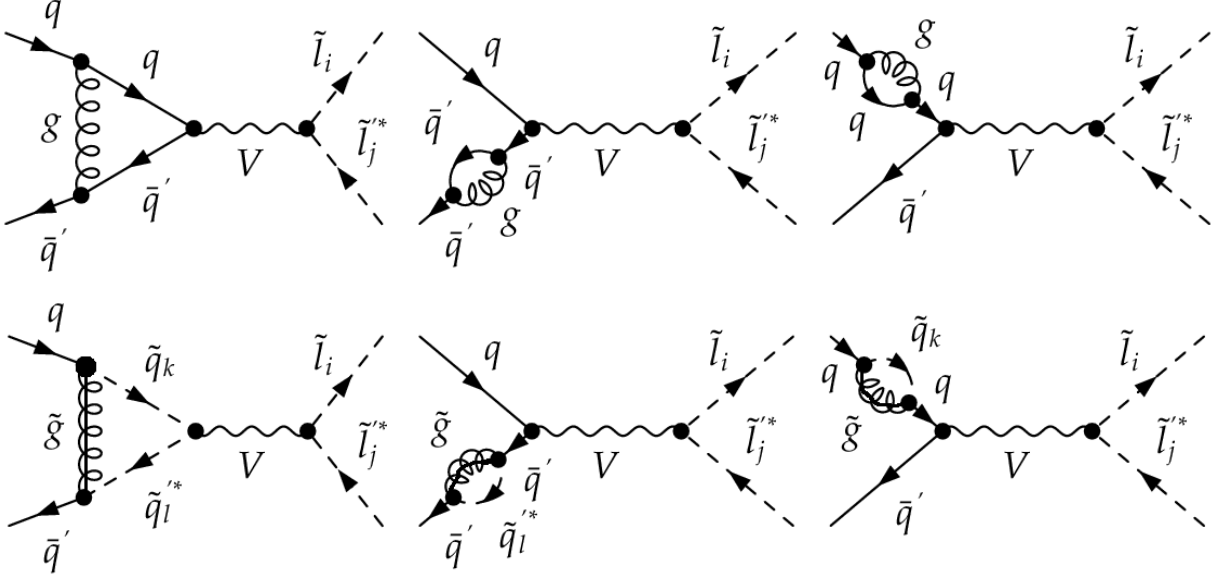


FIG. 2: Contributions of virtual diagrams for slepton-pair ($V = \gamma, Z^0$) and slepton-sneutrino associated ($V = W^\mp$) production at next-to-leading order in perturbative QCD. The first and second lines show the QCD and SUSY-QCD corrections, respectively. In the SUSY-QCD case, one has to sum over squark mass-eigenstates $k, l = 1, 2$.

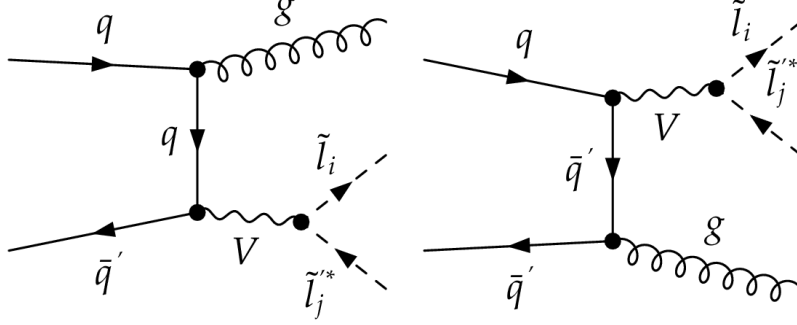


FIG. 3: Contributions from real gluon emission diagrams for slepton-pair ($V = \gamma, Z^0$) and slepton-sneutrino associated ($V = W^\mp$) production at next-to-leading order in perturbative QCD.

B. Next-to-Leading Order SUSY-QCD Corrections with Mixing Squark Loops

The NLO QCD and SUSY-QCD corrections to the slepton-pair production cross section have been studied for non-mixing sleptons in [18, 19]. At NLO in perturbative QCD, the quark-antiquark annihilation process receives contributions from virtual gluon exchange (see upper part of Fig. 2) and real gluon emission (see Fig. 3) diagrams, and we also have to take into account the quark-gluon initiated subprocess (see Fig. 4). The infrared and collinear singularities of the three-parton cross sections are extracted using the dipole subtraction formalism [28], and the virtual corrections have been evaluated in the $\overline{\text{MS}}$ renormalization scheme. For the SM QCD diagrams one has the well-known results [18, 29]

$$\sigma_{q\bar{q}^{(\prime)}}^{(1;\text{QCD})} \left(z, M^2; \frac{M^2}{\mu_F^2}, \frac{M^2}{\mu_R^2} \right) = \sigma_0^{(\prime)}(M^2) C_F \left[\left(\frac{\pi^2}{3} - 4 \right) \delta(1-z) + 4 \left(\frac{\ln(1-z)}{1-z} \right)_+ - \frac{1+z^2}{1-z} \ln z \right. \\ \left. - 2(1+z) \ln(1-z) + \frac{2P_{qq}^{(0)}(z)}{C_F} \ln \frac{M^2}{\mu_F^2} \right] \text{ and} \quad (13)$$

$$\sigma_{qg}^{(1;\text{QCD})} \left(z, M^2; \frac{M^2}{\mu_F^2}, \frac{M^2}{\mu_R^2} \right) = \sigma_0^{(\prime)}(M^2) T_R \left[\left(\frac{1}{2} - z + z^2 \right) \ln \frac{(1-z)^2}{z} + \frac{1}{4} + \frac{3z}{2} - \frac{7z^2}{4} + \frac{P_{qg}^{(0)}(z)}{T_R} \ln \frac{M^2}{\mu_F^2} \right], \quad (14)$$

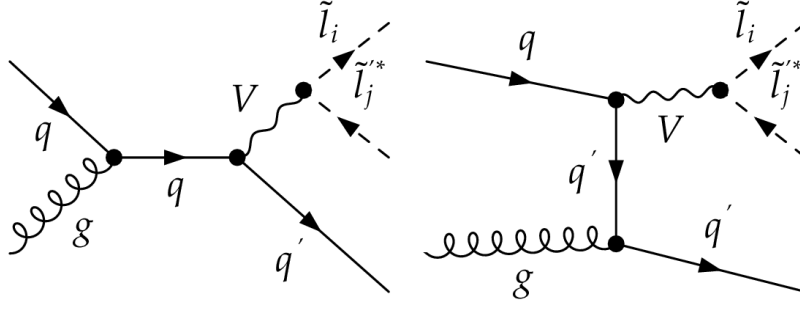


FIG. 4: Contributions from gg diagrams for slepton-pair ($V = \gamma, Z^0$) and slepton-sneutrino associated ($V = W^\mp$) production at next-to-leading order in perturbative QCD.

which expose the LO cross-sections $\sigma_0^{(l)}(M^2)$ in factorized form. $C_F = 4/3$ and $T_R = 1/2$ are the usual QCD colour factors, and $P_{qq}^{(0)}$ are the Altarelli-Parisi splitting functions [30]

$$P_{qq}^{(0)}(z) = \frac{C_F}{2} \left[\frac{3}{2} \delta(1-z) + \frac{2}{(1-z)_+} - (1+z) \right] \quad \text{and} \quad (15)$$

$$P_{qg}^{(0)}(z) = \frac{T_R}{2} [z^2 + (1-z)^2]. \quad (16)$$

We remind the reader that our normalization corresponds to a perturbative expansion in powers of α_s/π .

The three lower diagrams of Fig. 2 contain SUSY-QCD corrections. Generalizing results from [19] to the case of mixed squark mass eigenstates $k, l = 1, 2$ in the virtual loop diagrams, we obtain for neutral and charged currents

$$\begin{aligned} \sigma_{q\bar{q}}^{(1;\text{SUSY})} \left(z, M^2; \frac{M^2}{\mu_F^2}, \frac{M^2}{\mu_R^2} \right) &= \frac{\alpha^2 \pi C_F \beta^3}{36 M^2} \left[f_\gamma e_q^2 e_l^2 \delta_{ij} + f_{\gamma Z} \frac{e_q e_l \delta_{ij} \text{Re} [L_{Z\tilde{l}_i\tilde{l}_j} + R_{Z\tilde{l}_i\tilde{l}_j}]}{4 x_W (1-x_W) (1-m_Z^2/M^2)} \right. \\ &\quad \left. + f_Z \frac{|L_{Z\tilde{l}_i\tilde{l}_j} + R_{Z\tilde{l}_i\tilde{l}_j}|^2}{32 x_W^2 (1-x_W)^2 (1-m_Z^2/M^2)^2} \right] \delta(1-z) \quad \text{and} \quad (17) \end{aligned}$$

$$\sigma_{q\bar{q}'}^{(1;\text{SUSY})} \left(z, M^2; \frac{M^2}{\mu_F^2}, \frac{M^2}{\mu_R^2} \right) = \frac{\alpha^2 \pi C_F \beta^3}{36 M^2} \left[f_W \frac{|L_{W\tilde{l}_i\tilde{\nu}_l}|^2}{32 x_W^2 (1-x_W)^2 (1-m_W^2/M^2)^2} \right] \delta(1-z), \quad (18)$$

where now only the diagonal squared photon contribution to the Born cross section factorizes. The virtual loop coefficients $f_\gamma, f_{\gamma Z}, f_Z$ and f_W are given in App. B. Note that the quark mass, which appears in the off-diagonal mass matrix elements of the squarks running in the loops, corresponds to a linear Yukawa coupling in the superpotential and can not be neglected, even if it is much smaller than the total center-of-mass energy of the colliding partons allowing for a massless factorization inside the outer hadrons.

The full NLO contributions to the cross section are then given by

$$\sigma_{q\bar{q}^{(\prime)}}^{(1)} \left(z, M^2; \frac{M^2}{\mu_F^2}, \frac{M^2}{\mu_R^2} \right) = \sigma_{q\bar{q}^{(\prime)}}^{(1;\text{QCD})} \left(z, M^2; \frac{M^2}{\mu_F^2}, \frac{M^2}{\mu_R^2} \right) + \sigma_{q\bar{q}^{(\prime)}}^{(1;\text{SUSY})} \left(z, M^2; \frac{M^2}{\mu_F^2}, \frac{M^2}{\mu_R^2} \right) \quad \text{and} \quad (19)$$

$$\sigma_{qg}^{(1)} \left(z, M^2; \frac{M^2}{\mu_F^2}, \frac{M^2}{\mu_R^2} \right) = \sigma_{qg}^{(1;\text{QCD})} \left(z, M^2; \frac{M^2}{\mu_F^2}, \frac{M^2}{\mu_R^2} \right). \quad (20)$$

III. THRESHOLD RESUMMATION AT NEXT-TO-LEADING LOGARITHMIC ORDER

In this section, we recall some well-known results about soft-gluon resummation for the Drell-Yan process. The hadronic cross section in Eq. (6) can be written in factorized form in Mellin N -space as

$$\sigma(N, M^2) = \sum_{ab} f_{a/h_a}(N+1, \mu_F^2) f_{b/h_b}(N+1, \mu_F^2) \hat{\sigma}_{ab}(N, \alpha_s, M^2/\mu_R^2, M^2/\mu_F^2), \quad (21)$$

where the N -moments of the various quantities are defined according to the Mellin transform

$$F(N) = \int_0^1 dy y^{N-1} F(y), \quad (22)$$

with $y = \tau, z$, and $x_{a,b}$, respectively, for $F = \sigma, \hat{\sigma}$, and $f_{a,b}$.

A. Soft-Gluon Resummation in Mellin N -Space

The terms leading to finite and singular contributions in the threshold region are those proportional to $\delta(1-z)$ and to $\ln(1-z)$ and the plus-distributions in Eqs. (13) and (14). They respectively give rise to constant (N -independent) and to $(\ln N)/N$ and $\ln^i N$ ($i = 1, 2$) terms in Mellin space. [For a derivation of these correspondences we refer the reader, for instance, to App. A of [23].] These are the contributions that need to be resummed to all orders in perturbative QCD. In the following, we suppress the dependence on M^2/μ_R^2 and M^2/μ_F^2 for brevity.

The moments of the partonic cross section can be written in resummed form as [20, 21]

$$\hat{\sigma}_{ab}^{(\text{RES})}(N, \alpha_s) = \sigma_0^{(\prime)} C_{ab}(\alpha_s) \exp[S(N, \alpha_s)]. \quad (23)$$

The N -independent terms are collected in the C_{ab} functions

$$C_{q\bar{q}^{(\prime)}}(\alpha_s) = 1 + \sum_{n=1}^{\infty} \left(\frac{\alpha_s}{\pi}\right)^n C_{q\bar{q}^{(\prime)}}^{(n)}, \quad (24)$$

$$C_{qg}(\alpha_s) = \sum_{n=1}^{\infty} \left(\frac{\alpha_s}{\pi}\right)^n C_{qg}^{(n)}. \quad (25)$$

These contributions are mostly due to hard virtual corrections to the cross section, i.e. the terms proportional to $\delta(1-z)$ in Eqs. (13) and (14). The exponential form factor S can be written at NLL as

$$S(N, \alpha_s) = 2 \int_0^1 dz \frac{z^{N-1} - 1}{1-z} \int_{\mu_F^2}^{(1-z)^2 M^2} \frac{dq^2}{q^2} A(\alpha_s(q^2)). \quad (26)$$

The integrand in Eq. (26) embodies the contributions coming from the collinear emission of soft gluons from initial-state partons, i.e. the terms proportional to the plus-distributions in Eq. (13). It is a series expansion in the strong coupling constant,

$$A(\alpha_s) = \sum_{n=1}^{\infty} \left(\frac{\alpha_s}{\pi}\right)^n A_n, \quad (27)$$

whose coefficients are perturbatively computable through a fixed-order calculation. In particular, it has been proven [31] that in the $\overline{\text{MS}}$ factorization scheme the coefficients of the A -function are exactly equal to the large- N coefficients of the diagonal splitting function

$$\gamma_{qq}(\alpha_s) = \int_0^1 dz z^{N-1} P_{qq}(z) = -A(\alpha_s) \ln \bar{N} + \mathcal{O}(1), \quad (28)$$

where $\bar{N} = N \exp[\gamma_E]$ and $\gamma_E = 0.5772\dots$ is the Euler-Mascheroni constant. Performing the integration in Eq. (26) and using Eq. (27), we obtain the form factor up to NLL,

$$S(N, \alpha_s) = g_1(\lambda) \ln \bar{N} + g_2(\lambda). \quad (29)$$

The functions g_1 and g_2 resum the LL ($\alpha_s^n \ln^{n+1} N$) and NLL ($\alpha_s^n \ln^n N$) contributions, respectively, and are given by [20, 21]

$$g_1(\lambda) = \frac{A_1}{\beta_0 \lambda} [2\lambda + (1-2\lambda) \ln(1-2\lambda)] \quad \text{and} \quad (30)$$

$$g_2(\lambda) = \frac{A_1 \beta_1}{\beta_0^3} \left[2\lambda + \ln(1-2\lambda) + \frac{1}{2} \ln^2(1-2\lambda) \right] - \frac{A_2}{\beta_0^2} [2\lambda + \ln(1-2\lambda)] \\ + \frac{A_1}{\beta_0} [2\lambda + \ln(1-2\lambda)] \ln \frac{M^2}{\mu_R^2} - \frac{2A_1 \lambda}{\beta_0} \ln \frac{M^2}{\mu_F^2}, \quad (31)$$

where $\lambda = [\beta_0 \alpha_s \ln \bar{N}]/\pi$. The first two coefficients of the QCD β -function are

$$\beta_0 = \frac{1}{12}(11 C_A - 2 N_f) \quad \text{and} \quad \beta_1 = \frac{1}{24}(17 C_A^2 - 5 C_A N_f - 3 C_F N_f), \quad (32)$$

N_f being the number of effectively massless quark flavours and $C_F = 4/3$, $C_A = 3$ the usual QCD colour factors.

Thus, the knowledge of the first two coefficients of the function $A(\alpha_s)$ [32, 33],

$$A_1 = C_F \quad \text{and} \quad A_2 = \frac{1}{2} C_F \left[C_A \left(\frac{67}{18} - \frac{\pi^2}{6} \right) - \frac{5}{9} N_f \right], \quad (33)$$

together with the first coefficients of the C -functions in Eqs. (24) and (25),

$$C_{q\bar{q}^{(\prime)}}^{(1)} = C_F \left(\frac{2\pi^2}{3} - 4 + \frac{3}{2} \ln \frac{M^2}{\mu_F^2} \right) \quad \text{and} \quad (34)$$

$$C_{qg}^{(1)} = 0, \quad (35)$$

allows us to perform resummation up to NLL.

B. Improvements of the Resummation Formalism

In the limit of large N , the cross section is clearly dominated by terms of $\mathcal{O}(\ln^2 N)$, $\mathcal{O}(\ln N)$ and $\mathcal{O}(1)$. It seems thus reasonable to neglect terms suppressed by powers of $1/N$ in the resummation formalism. Actually these last terms are multiplied by powers of $\ln N$ and could as well provide a non-negligible effect in the threshold limit. In [35, 36] it has been shown that these contributions are due to collinear parton emission and can be consistently included in the resummation formula, leading to a ‘‘collinear-improved’’ resummation formalism. The modification simply amounts to the introduction of an N -dependent term in the $C_{q\bar{q}^{(\prime)}}^{(1)}$ and $C_{qg}^{(1)}$ coefficient of Eqs. (34) and (35)

$$C_{q\bar{q}^{(\prime)}}^{(1)} \rightarrow \tilde{C}_{q\bar{q}^{(\prime)}}^{(1)} = C_{q\bar{q}^{(\prime)}}^{(1)} + 2 A_1 \frac{\ln \bar{N} - \frac{1}{2} \ln \frac{M^2}{\mu_f^2}}{N}, \quad (36)$$

$$C_{qg}^{(1)} \rightarrow \tilde{C}_{qg}^{(1)} = C_{qg}^{(1)} - T_R \frac{\ln \bar{N} - \frac{1}{2} \ln \frac{M^2}{\mu_f^2}}{N}. \quad (37)$$

Furthermore, the exponentiation of the contributions embodied in the C -function has been proved in [37], leading to the following modification in Eq. (23):

$$\hat{\sigma}_{ab}^{(\text{RES})}(N, \alpha_s) = \sigma_0^{(\prime)} \exp \left[C_{q\bar{q}^{(\prime)}}^{(1)}(\alpha_s) \right] \exp \left[S(N, \alpha_s) \right]. \quad (38)$$

As the authors of Ref. [37] recognize, this exponentiation of the N -independent terms is not comparable to the standard threshold resummation in terms of predictive power. While in the latter case a low-order calculation can be used to predict the behaviour of full towers of logarithms, in the former case it is not possible to directly get information on the behaviour of constant terms at, say, n loops, but a complete calculation at the n^{th} perturbative order will still be necessary. Nonetheless, the comparison of the numerical results obtained with and without the exponentiation of the constant terms can at least provide an estimate of the errors due to missing higher-order corrections.

C. Inverse Mellin-Transform and Matching Procedure

Once resummation has been achieved in N -space, an inverse Mellin-transform back to the physical x -space is needed. The customary way to perform this inversion, avoiding the singularities of the N -moments, is the ‘‘Minimal Prescription’’ of [34],

$$\sigma = \frac{1}{2\pi i} \int_{C_{MP}-i\infty}^{C_{MP}+i\infty} dN \left(\frac{M^2}{S} \right)^{-N} \sigma(N, M^2). \quad (39)$$

The constant C_{MP} has to be chosen so that all the poles in the integrand are to the left of the integration contour in the complex N -plane except for the Landau pole at $N = \exp[\pi/(2\beta_0 \alpha_s)]$, which should lie far to the right on the real axis.

Finally, a matching procedure of the NLL resummed cross section to the NLO result has to be performed in order to keep the full information contained in the fixed-order calculation and to avoid possible double-counting of the logarithmic enhanced contributions. A correct matching is achieved through

$$\sigma = \sigma^{(\text{F.O.})} + \frac{1}{2\pi i} \int_{C_{MP-i\infty}}^{C_{MP+i\infty}} dN \left(\frac{M^2}{S} \right)^{-N} \left[\sigma^{(\text{RES})}(N, M^2) - \sigma^{(\text{EXP})}(N, M^2) \right], \quad (40)$$

where $\sigma^{(\text{F.O.})}$ is the fixed-order perturbative result, $\sigma^{(\text{RES})}$ is the resummed cross section, and $\sigma^{(\text{EXP})}$ is the truncation of the resummed cross section to the same perturbative order as $\sigma^{(\text{F.O.})}$. In our case the expansion of the resummed partonic cross section up to order α_s reads

$$\hat{\sigma}_{q\bar{q}^{(\prime)}}^{(\text{EXP})}(N, M^2) = \sigma_0^{(\prime)}(M^2) \left[1 + \frac{\alpha_s}{\pi} \left(C_F \left(2 \ln^2 \bar{N} - 2 \ln \bar{N} \ln \frac{M^2}{\mu_F^2} \right) + \tilde{C}_{q\bar{q}^{(\prime)}}^{(1)} \right) \right] + \mathcal{O}(\alpha_s^2) \quad \text{and} \quad (41)$$

$$\hat{\sigma}_{qg}^{(\text{EXP})}(N, M^2) = \sigma_0^{(\prime)}(M^2) \left[\frac{\alpha_s}{\pi} \tilde{C}_{qg}^{(1)} \right] + \mathcal{O}(\alpha_s^2). \quad (42)$$

In Mellin-space, the fixed order NLO cross sections of Eqs. (13) and (14) read [38]

$$\begin{aligned} \hat{\sigma}_{q\bar{q}^{(\prime)}}^{(\text{F.O.})}(N, M^2) &= \sigma_0^{(\prime)}(M^2) \left[1 + \frac{\alpha_s}{\pi} C_F \left(4 S_1^2(N) - \frac{4}{N(N+1)} S_1(N) + \frac{2}{N^2} + \frac{2}{(N+1)^2} \right. \right. \\ &\quad \left. \left. - 8 + \frac{4\pi^2}{3} + \left[\frac{2}{N(N+1)} + 3 - 4 S_1(N) \right] \ln \frac{M^2}{\mu_F^2} \right) \right] + \mathcal{O}(\alpha_s^2) \quad \text{and} \quad (43) \end{aligned}$$

$$\begin{aligned} \hat{\sigma}_{qg}^{(\text{F.O.})}(N, M^2) &= \sigma_0^{(\prime)}(M^2) \left[\frac{\alpha_s}{\pi} T_R \left(-2 \frac{N^2 + N + 2}{N(N+1)(N+2)} S_1(N) + \frac{N^4 + 11N^3 + 22N^2 + 14N + 4}{N^2(N+1)^2(N+2)^2} \right. \right. \\ &\quad \left. \left. + \frac{N^2 + N + 2}{N(N+1)(N+2)} \ln \frac{M^2}{\mu_F^2} \right) \right] + \mathcal{O}(\alpha_s^2) \quad (44) \end{aligned}$$

with $S_1(N) = \sum_{j=1}^N 1/j$. In the large- N limit, $S_1(N) \simeq \ln \bar{N} + 1/(2N)$, and we get

$$\hat{\sigma}_{q\bar{q}^{(\prime)}}^{(\text{F.O.})}(N, M^2) = \sigma_0^{(\prime)}(M^2) \left[1 + \frac{\alpha_s}{\pi} \left(C_F \left(2 \ln^2 \bar{N} - 2 \ln \bar{N} \ln \frac{M^2}{\mu_F^2} \right) + \tilde{C}_{q\bar{q}^{(\prime)}}^{(1)} \right) \right] + \mathcal{O}(\alpha_s^2) \quad \text{and} \quad (45)$$

$$\hat{\sigma}_{qg}^{(\text{F.O.})}(N, M^2) = \sigma_0^{(\prime)}(M^2) \left[\frac{\alpha_s}{\pi} \tilde{C}_{qg}^{(1)} \right] + \mathcal{O}(\alpha_s^2). \quad (46)$$

Comparing Eqs. (41), (42), (45), and (46), we see that the expansion of the resummed cross section at order α_s correctly reproduces the fixed order result in the large- N limit, including even terms that are suppressed by $1/N$.

IV. NUMERICAL RESULTS

For the masses and widths of the electroweak gauge bosons, we use the current values of $m_Z = 91.1876$ GeV, $m_W = 80.403$ GeV, $\Gamma_Z = 2.4952$ GeV, and $\Gamma_W = 2.141$ GeV. The CKM-matrix elements are computed using

$$V = \begin{pmatrix} c_{12}c_{13} & s_{12}c_{13} & s_{13}e^{-i\delta} \\ -s_{12}c_{23} - c_{12}s_{23}s_{13}e^{i\delta} & c_{12}c_{23} - s_{12}s_{23}s_{13}e^{i\delta} & s_{23}c_{13} \\ s_{12}s_{23} - c_{12}c_{23}s_{13}e^{i\delta} & -c_{12}s_{23} - s_{12}c_{23}s_{13}e^{i\delta} & c_{23}c_{13} \end{pmatrix} \quad (47)$$

with $s_{ij} = \sin \theta_{ij}$ and $c_{ij} = \cos \theta_{ij}$, θ_{ij} being the usual angles relative to the mixing of two specific generations i and j and δ being the CP-violating complex phase. Their average values are given by

$$s_{12} = 0.2243, \quad s_{23} = 0.0413, \quad s_{13} = 0.0037, \quad \text{and} \quad \delta = 1.05. \quad (48)$$

The squared sine of the electroweak mixing angle

$$\sin^2 \theta_W = 1 - m_W^2/m_Z^2 \quad (49)$$

and the electromagnetic fine structure constant

$$\alpha = \sqrt{2}G_F m_W^2 \sin^2 \theta_W / \pi \quad (50)$$

can be calculated in the improved Born approximation using the world average value of $G_F = 1.16637 \cdot 10^{-5} \text{ GeV}^{-2}$ for Fermi's coupling constant [12].

The physical masses of the SUSY particles and the mixing angles are computed with the computer program SUSPECT [39], including a consistent calculation of the Higgs mass, with all one-loop and the dominant two-loop radiative corrections in the renormalization group equations that link the restricted set of SUSY-breaking parameters at the gauge coupling unification scale to the complete set of observable SUSY masses and mixing angles at the electroweak scale. We choose one minimal supergravity (mSUGRA) point, SPS 1a, and one gauge-mediated supersymmetry breaking (GMSB) point, SPS 7, as benchmarks for our numerical study [40]. SPS 1a is a typical mSUGRA point with an intermediate value of $\tan \beta = 10$ and $\mu > 0$. It has a model line attached to it, which is specified by $m_0 = -A_0 = 0.4 m_{1/2}$. For $m_{1/2} = 250 \text{ GeV}$, this SUSY-breaking scenario leads to light sleptons $\tilde{\tau}_1, \tilde{e}_1, \tilde{\tau}_2, \tilde{e}_2, \tilde{\nu}_\tau$ and $\tilde{\nu}_e$ with masses of 136.2, 146.4, 216.3, 212.3, 196.1 and 197.1 GeV and to heavy squarks with masses around 500-600 GeV [46]. SPS 7 is a GMSB scenario with a $\tilde{\tau}_1$ as the next-to-lightest SUSY particle (NLSP) and an effective SUSY-breaking scale $\Lambda = 40 \text{ TeV}$, $N_{\text{mes}} = 3$ messenger fields of mass $M_{\text{mes}} = 80 \text{ TeV}$, $\tan \beta = 15$, and $\mu > 0$, which leads again to light sleptons with masses of 114.8, 121.1, 263.9, 262.1, 249.5 and 249.9 GeV, respectively, and even heavier squarks with masses around 800-900 GeV. Its model line is defined by $M_{\text{mes}} = 2\Lambda$. The slepton masses and mixing angles are actually quite similar for the SPS 1a mSUGRA and SPS 7 GMSB points, so that the corresponding production cross sections will not differ significantly. Slepton detection will, however, be slightly different in both scenarios, as the sleptons decay to a relatively massive neutralino ($\tilde{\chi}_1^0$) lightest SUSY particle (LSP) at SPS 1a, but to a very light gravitino LSP at SPS 7. The lightest tau slepton thus decays into a tau lepton and missing transverse energy. Feasibility studies of tau-slepton identification at the LHC with the ATLAS detector [41] and tau tagging with the CMS detector [42] have recently shown that stau masses should be observable up to the TeV range.

Our cross sections are calculated for the Tevatron $p\bar{p}$ -collider, currently operating at $\sqrt{S} = 1.96 \text{ TeV}$, as well as for the LHC pp -collider, bound to operate at $\sqrt{S} = 14 \text{ TeV}$ starting in 2008. For the LO (NLO and NLL) predictions, we use the LO 2001 [43] (NLO 2004 [44]) MRST-sets of parton distribution functions (PDFs). For the NLO and NLL predictions, α_s is evaluated with the corresponding value of $\Lambda_{\overline{\text{MS}}}^{n_f=5} = 255 \text{ MeV}$ at two-loop accuracy. We fix the unphysical scales μ_F and μ_R equal to the invariant mass M of the slepton (slepton-sneutrino) pair.

A. Invariant-Mass Distributions for Slepton Pairs

The invariant-mass distribution $M^3 d\sigma/dM$ for first- (and equal-mass second-) generation sleptons at the Tevatron is shown in Fig. 5 (top), the one for (slightly lighter) third-generation sleptons at the LHC in Fig. 5 (bottom). In both cases, we have chosen the SPS 7 GMSB benchmark point. The differential cross section $d\sigma/dM$ has been multiplied by a factor M^3 in order to remove the leading mass dependence of propagator and phase space factors. As is to be expected for P -wave production of scalar particles, the distributions rise above the threshold at $\sqrt{S} = 2m_{\tilde{l}}$ with the third power of the slepton velocity β , see Eq. (9), and peak at about 100 GeV above threshold (at 370 GeV for $M^3 d\sigma/dM$ and 310 GeV for $d\sigma/dM$ for the Tevatron; 410 GeV and 300 GeV for the LHC), before falling off steeply due to the s -channel propagator and the decreasing parton luminosity. As can also be seen from Eqs. (13) and (14), the QCD corrections do not alter the P -wave velocity dependence close to threshold. At the Tevatron, the total and NLO SUSY-QCD predictions exceed the maximal LO cross section by 36 and 31%, respectively, whereas at the LHC, the maximal cross section increases by 28 and 27%. Threshold resummation effects are thus clearly more important at the Tevatron, where the hadronic center-of-mass energy is limited and the scaling variable $\tau = M^2/S$ is closer to one, and they increase with M to the right of both plots. The maximal theoretical error is estimated in Fig. 5 by an independent variation of the factorization and renormalization scales between $M/2$ and $2M$. It is indicated as a shaded, vertically, and horizontally hatched band for the LO, NLO SUSY-QCD, and the total prediction. At LO, the only dependence comes from the factorization scale. It increases with the momentum-fraction x of the partons in the proton or anti-proton and is therefore already substantial for small M at the Tevatron, but only for larger M at the LHC. At NLO, this dependence is reduced due to the factorization of initial-state singularities, but a strong additional dependence is introduced by the renormalization scale in the coupling $\alpha_s(\mu_R)$. After resummation, this dependence is reduced as well, so that the total scale uncertainty at the Tevatron diminishes from 20%–35% for NLO to only 16%–17% for the matched resummed result. The reduction is, of course, more important in the large- M region. At the LHC, where α_s is evaluated at a larger renormalization scale and is thus less sensitive to it, the corresponding numbers are 18%–25% and 15%–17%.

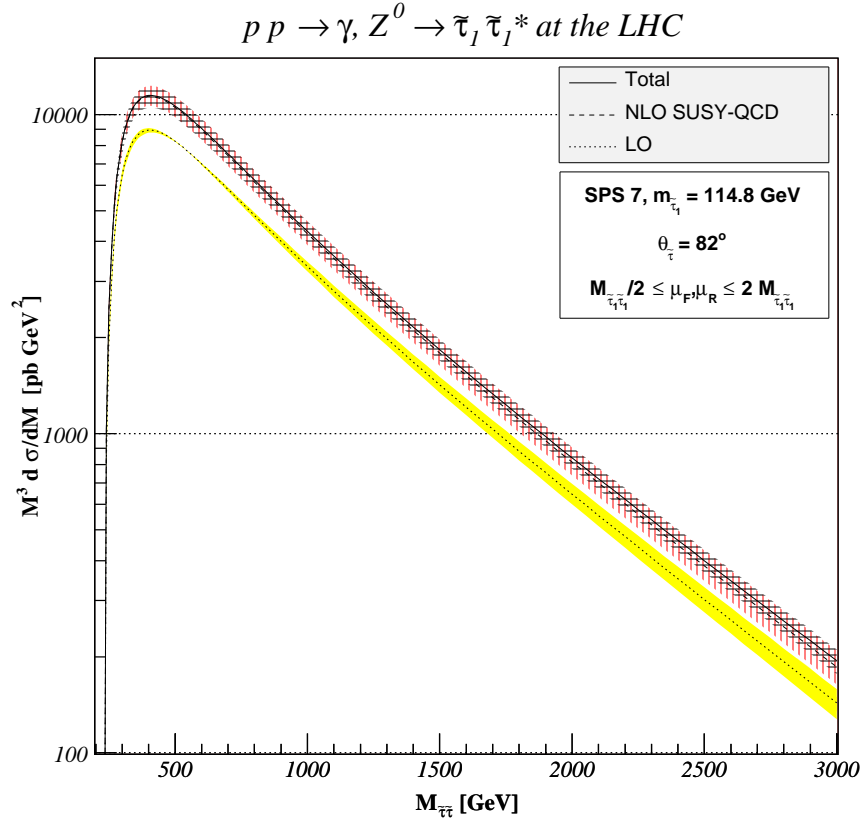
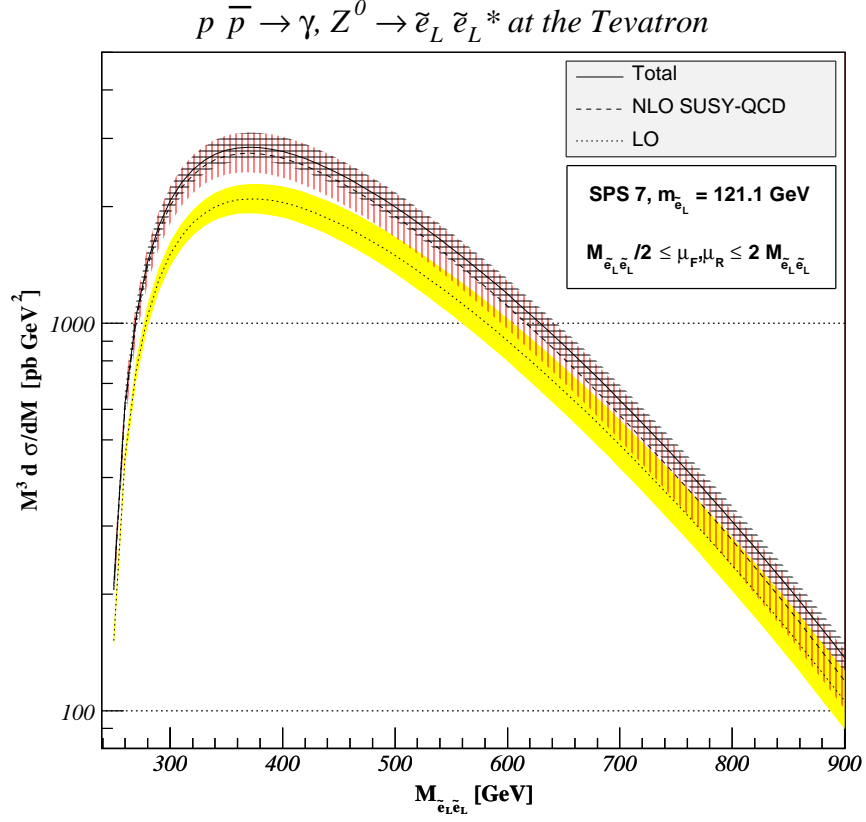


FIG. 5: Invariant-mass distribution $M^3 d\sigma/dM$ of \tilde{e}_L -pairs at the Tevatron (top) and $\tilde{\tau}_1$ -pairs at the LHC (bottom) for the benchmark point SPS 7. We show the total NLL+NLO matched and the fixed order NLO SUSY-QCD and LO QCD results, including the respective scale uncertainties as horizontally hatched, vertically hatched and shaded bands.

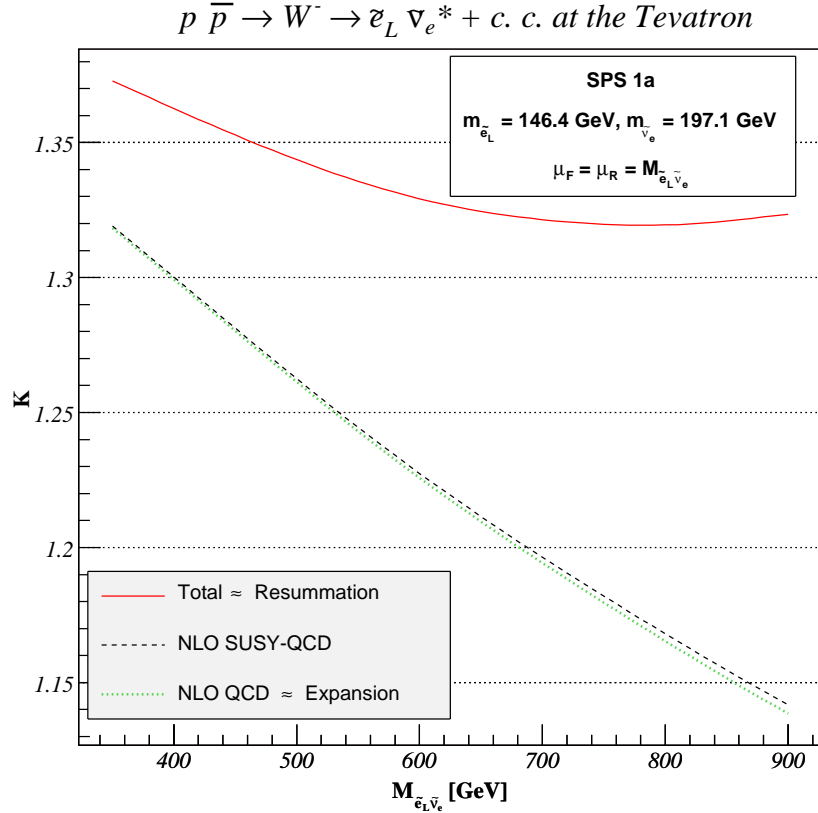
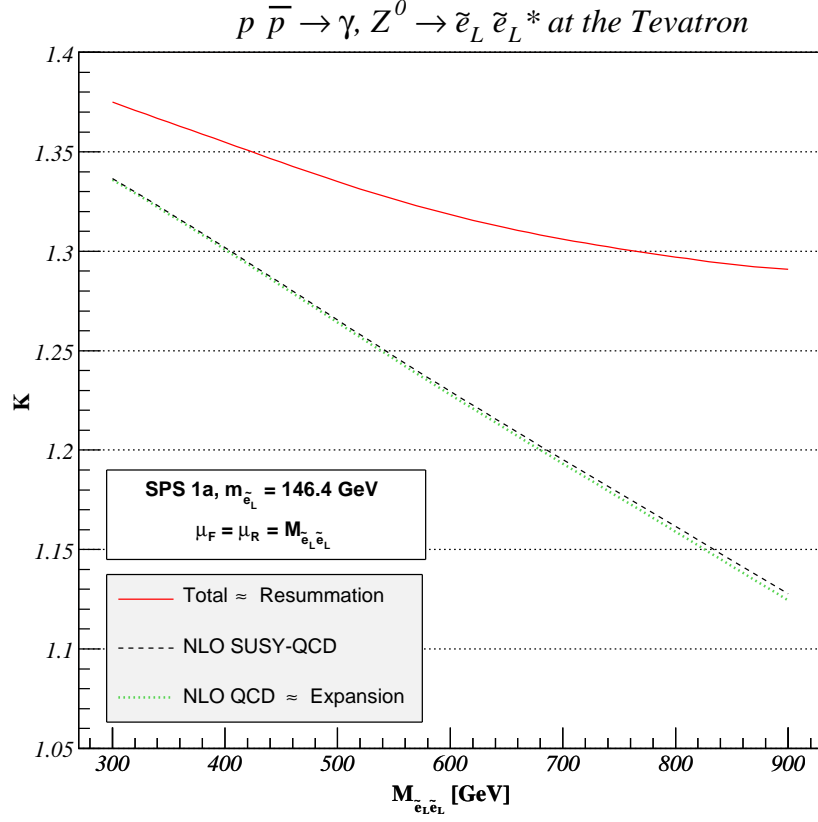


FIG. 6: K -factors as defined in Eq. (51) for $\tilde{\nu}_L$ -pair (top) and associated $\tilde{\nu}_L \tilde{\nu}_e^*$ production (bottom) at the Tevatron for the benchmark point SPS 1a. We show the total NLL+NLO matched result, which is almost identical to the purely resummed result at NLL, as well as the fixed order NLO SUSY-QCD and QCD results. The latter practically coincides with the resummed result expanded up to NLO.

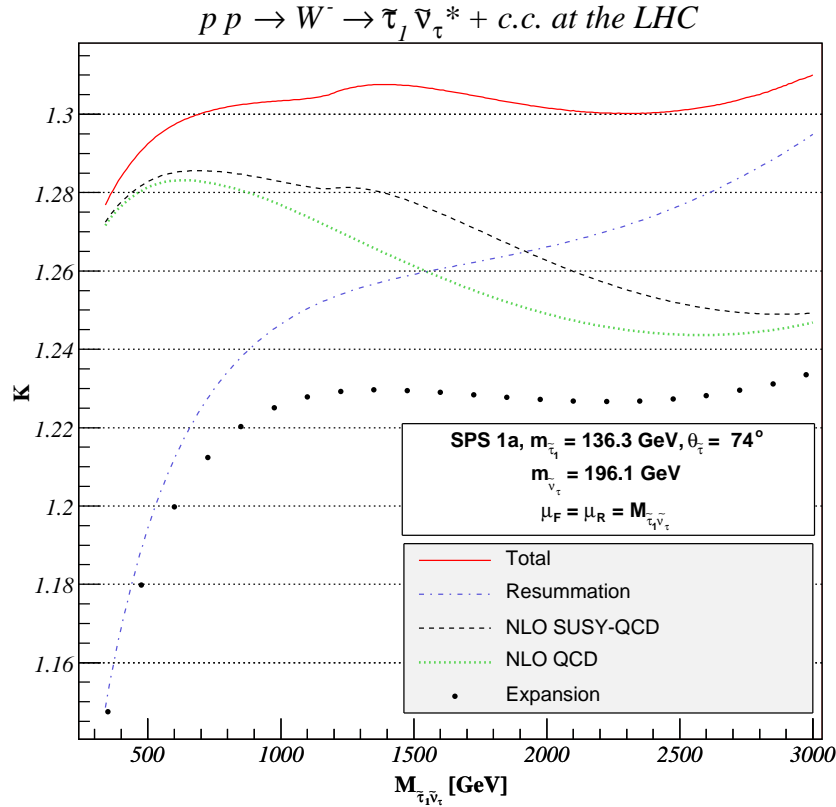
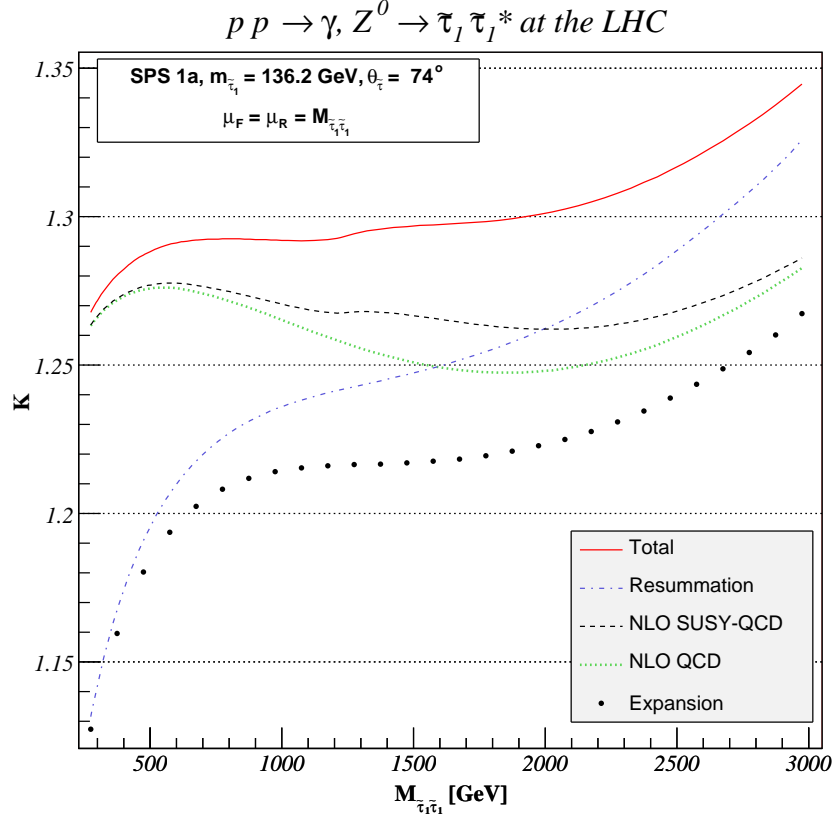


FIG. 7: K -factors as defined in Eq. (51) for $\tilde{\tau}_1$ -pair (top) and associated $\tilde{\tau}_1 \tilde{\nu}_\tau^*$ production (bottom) at the LHC for the benchmark point SPS 1a. We show the total NLL+NLO matched result, the resummed result at NLL, the fixed order NLO SUSY-QCD and QCD results, and the resummed result expanded up to NLO.

For the mSUGRA scenario SPS 1a, with nonetheless similar slepton masses and mixing angles (see above), we show in Figs. 6 and 7 the cross section correction factors

$$K^i = \frac{d\sigma^i/dM}{d\sigma^{\text{LO}}/dM}, \quad (51)$$

where i labels the corrections induced by NLO QCD (Eqs. (13) and (14)), additional NLO SUSY-QCD (Eqs. (19) and (20)), resummation (Eqs. (23), (36), and (37)), and the matched total contributions (Eq. (40)) as well as the fixed-order expansion (Eqs. (41) and (42)) of the resummation contribution as a function of the invariant mass M . As one can see immediately, the mass-dependence of these corrections for charged-current associated production of sleptons and sneutrinos (lower parts of Figs. 6 and Fig. 7) does not differ substantially from the mass-dependence of the neutral-current production of slepton-pairs (upper parts).

At the Tevatron (Fig. 6), where we are close to the threshold, resummation effects are already important at low M (4%) and increase to sizeable 16% at large M . The NLO QCD result is thus dominated by large logarithms and coincides with the expanded result at the permille level. In addition, the relative importance of the (finite) SUSY-QCD contributions is reduced, and the total prediction coincides with the resummed prediction, since fixed-order and expanded contributions cancel each other in Eq. (40). We have also verified that exponentiating the finite (N -independent) terms collected in the coefficient function $C_{q\bar{q}(\nu)}^{(1)}$, as proposed in [37] (see Eq. 38), leads only to a 0.6%–0.8% increase of the matched resummed result. The Tevatron being a $p\bar{p}$ -collider, the total cross section is dominated by $q\bar{q}$ -annihilation, and qg -scattering contributes at most 1% at small M (or small x), where the gluon density is still appreciable. Integration over M leads to total cross sections for the neutral (charged) current processes in Fig. 6 of 4.12 (3.92) fb in LO, 5.3 (4.96) fb in NLO (SUSY-)QCD, and 5.55 (5.28) fb for the matched resummed calculation. The corresponding (global) K -factors

$$K_{\text{glob}}^i = \frac{\sigma^i}{\sigma^{\text{LO}}} = \frac{\int dM d\sigma^i / dM}{\int dM d\sigma^{\text{LO}} / dM} \quad (52)$$

are then 1.29 (1.27) at fixed-order and 1.35 (1.35) with resummation.

At the LHC (Fig. 7), sleptons can be produced with relatively small invariant mass M compared to the total available center-of-mass energy \sqrt{S} , so that $z = \tau/(x_a x_b) = M^2/s \ll 1$ and the resummation of $(1-z)$ -logarithms is less important. This is particularly true for the production of the light mass-eigenstates of mixing third-generation sleptons, as shown in Fig. 7. In the low- M (left) parts of these plots, the total result is less than 0.5% larger than the NLO (SUSY-)QCD result. Only at large M the logarithms become important and lead to a 7% increase of the K -factor with resummation over the fixed-order result. In this region, the resummed result approaches the total prediction, since the NLO QCD calculation is dominated by large logarithms and approaches the expanded resummed result. However, we are still far from the hadronic threshold region, so that both resummed and fixed-order contributions and a consistent matching of the two are needed. At low M , where finite terms dominate, the resummed contribution is close to its fixed-order expansion and disappears with M . In the intermediate- M region, one can observe the effect of SUSY-QCD contributions, in particular the one coming from the $\tilde{q}\tilde{q}\tilde{g}$ -vertex correction (lower left diagram in Fig. 2). As $M \geq 2m_{\tilde{q}}$, one crosses the threshold for squark-pair production and observes a resonance in Fig. 7. As for the Tevatron, exponentiating the finite (N -independent) terms collected in the coefficient function $C_{q\bar{q}(\nu)}^{(1)}$ leads only to a 1% increase of the matched resummed result. The LHC being a high-energy pp -collider, it has a significant gluon-luminosity, in particular at small M (or x), and indeed the qg -subprocess changes (lowers) the total cross section by 7% at small M and 3% at large M . After integration over M , we obtain total cross sections of 27 (9.59) fb in LO, 34.3 (12.3) fb in NLO SUSY-QCD, and 34.6 (12.5) fb for the resummed-improved result, corresponding to global K -factors of 1.28 for fixed-order and 1.29 for the matched resummed cross section for both processes. Resummation of large logarithms is thus not as important as for the Tevatron at the benchmark point SPS 1a.

B. Scale Variations of the Total Cross Section

In this section, we study the dependence of total, i.e. invariant-mass integrated, slepton-pair and slepton-sneutrino cross sections on three different scales: first the dependence on the effective SUSY-breaking scale Λ as defined in the GMSB model line SPS 7, and then the dependence on the renormalization and factorization scales $\mu_{R,F}$ at the point SPS 7. We remind the reader that the model line for SPS 7 is $M_{\text{mes}} = 2\Lambda$ with $N_{\text{mes}} = 3$, $\tan\beta = 15$, and $\mu > 0$ fixed. The benchmark point at $\Lambda = 40$ TeV will be indicated in the figures where Λ varies as a vertical dashed line, and we show in addition to the scale Λ the mass scale of the produced charged slepton, ranging from 80 (87.5) to 280 (385) GeV for \tilde{e}_L ($\tilde{\tau}_1$).

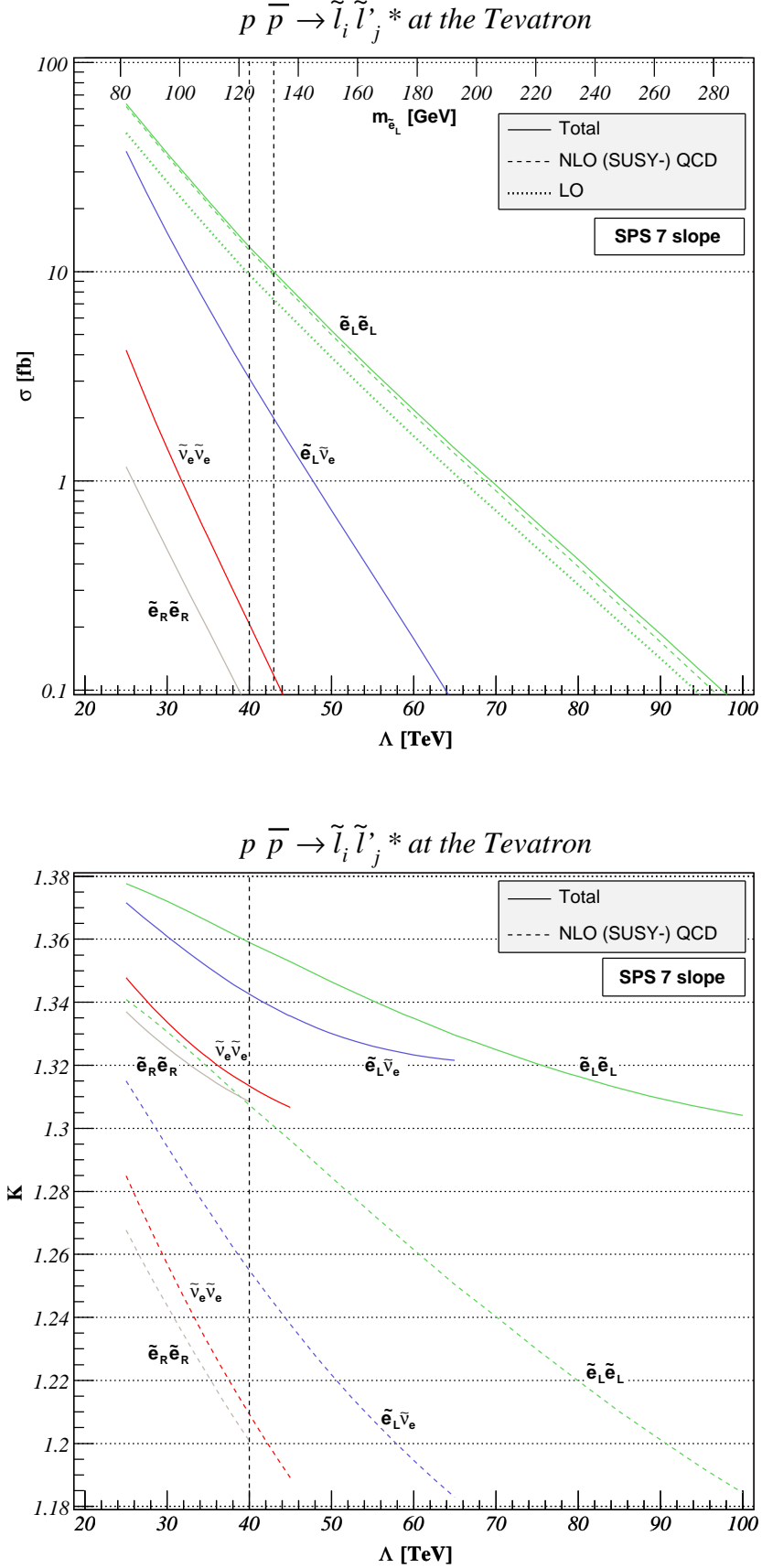


FIG. 8: Total cross sections (top) and K -factors as defined in Eq. (52) (bottom) for first- (and second-) generation slepton-pair and slepton-sneutrino associated production at the Tevatron along the model line attached to the SPS 7 benchmark point (vertical dashed line). We show the total NLL+NLO matched and the fixed order NLO (SUSY-)QCD and LO QCD results.

In Fig. 8, total cross sections (top) and K -factors (bottom) are shown at the Tevatron, which is expected to produce a total integrated luminosity of $4\text{--}8\text{ fb}^{-1}$. Only left-handed (charged) eigenstates couple to the weak (electromagnetic) neutral current, so that their respective cross sections are enhanced. However, even for \tilde{e}_L -pair production the mass-range is limited to masses below 280 GeV, where the cross section reaches 0.1 fb and at most one event would be produced. NLO and resummation corrections are clearly important, as they increase the LO prediction by 18 to 28% (lower part of Fig. 8). At the SPS 7 benchmark point, the corrections would thus induce a shift in the selectron mass as deduced from a total cross section measurement by about 8 GeV (cf. the two dashed lines in the upper part of Fig. 8). By comparing the NLO and total predictions, one observes an increased importance of threshold resummation for heavier sleptons, as expected.

At the LHC (Fig. 9), even very heavy sleptons can be detected (see above), but we restrict ourselves to the range $\Lambda \leq 135\text{ TeV}$. The NLO and resummed corrections are again large (25–30%), but the resummation corrections only become appreciable for large SUSY-breaking scales (or slepton masses). The largest cross section is obtained for pair production of the light stau mass eigenstate, even though it has a large right-handed component. Conversely, the heavier stau mass eigenstate has a large left-handed component, so that its cross section is less suppressed. At the SPS 7 benchmark point, the corrections would again induce a shift in the slepton ($\tilde{\tau}_1$) mass as deduced from a total cross section measurement by about 8 GeV (cf. the two dashed lines in the upper part of Fig. 9).

Finally, we consider the theoretical uncertainty of invariant-mass integrated total cross sections at the Tevatron (Fig. 10) and the LHC (Fig. 11) as induced by variations of the factorization scale (top), renormalization scale (middle), or both (bottom). The μ_R -dependence (middle), which is absent in LO, is first introduced in NLO, but then tamed by the resummation procedure. On the other hand, the logarithmic μ_F -dependence (top), already present through the PDFs at LO, is overcompensated (reduced) at NLO for the LHC (Tevatron) and then (further) stabilized by resummation. This works considerably better at the LHC, where at least one quark PDF is sea-like and the PDFs are evaluated at lower x , than at the Tevatron, where both PDFs can be valence-like and are evaluated at relatively large x . In total, the theoretical uncertainty at the Tevatron (LHC), defined by the ratio of the cross section difference at $\mu_F = \mu_R = m_{\tilde{l}}/2$ and $\mu_F = \mu_R = 2m_{\tilde{l}}$ over their sum, increases from 20 (7) % in LO to 29 (17) % in NLO, but is then reduced again to 23 (8) % for the resummed-improved prediction.

V. CONCLUSIONS

In summary, we have presented a first and extensive study on threshold resummation effects for SUSY-particle production at hadron colliders, focusing on Drell-Yan like slepton-pair and slepton-sneutrino associated production in mSUGRA and GMSB scenarios. After confirming the known NLO QCD corrections and generalizing the NLO SUSY-QCD corrections to the case of mixing squarks in the virtual loop contributions, we employed the usual Mellin N -space resummation formalism with the minimal prescription for the inverse Mellin-transform, but improved it by resumming $1/N$ -suppressed and a class of N -independent universal contributions. Numerically, our results increase the theoretical cross sections by 5 to 15% with respect to the NLO prediction and stabilize them by reducing the scale dependence from up to 20% at NLO to less than 10% with threshold resummation.

Acknowledgments

We thank M. Cacciari for useful discussions concerning the numerical stability of parton density parameterizations in Mellin N -space. This work was supported by a CNRS/IN2P3 postdoctoral grant and a Ph.D. fellowship of the French ministry for education and research.

APPENDIX A: SFERMION MIXING

The soft SUSY-breaking terms A_f of the trilinear Higgs-sfermion-sfermion interaction and the off-diagonal Higgs mass parameter μ in the MSSM Lagrangian induce mixings of the left- and right-handed sfermion eigenstates $\tilde{f}_{L,R}$ of the electroweak interaction into mass eigenstates $\tilde{f}_{1,2}$. The sfermion mass matrix is given by [2]

$$\mathcal{M}^2 = \begin{pmatrix} m_{LL}^2 + m_f^2 & m_f m_{LR}^* \\ m_f m_{LR} & m_{RR}^2 + m_f^2 \end{pmatrix} \quad (\text{A1})$$

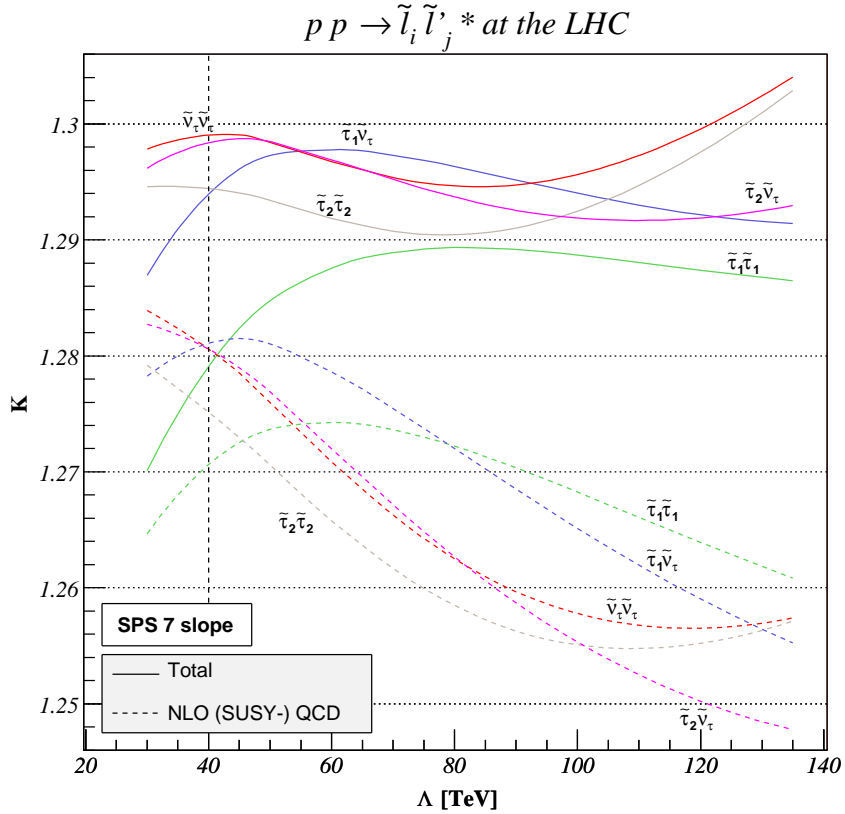
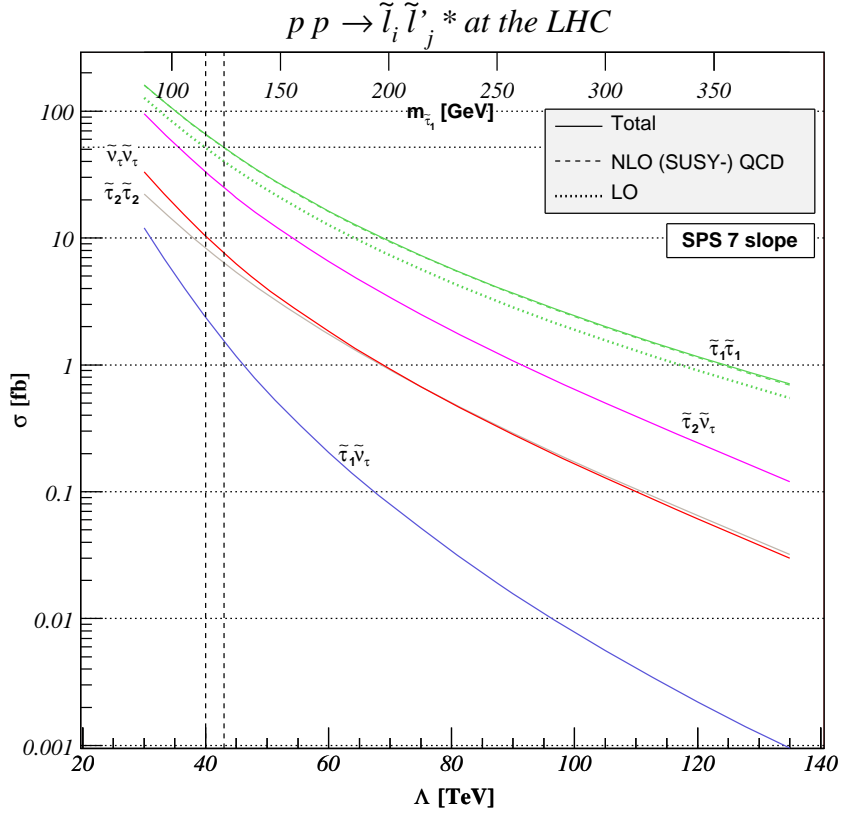


FIG. 9: Total cross sections (top) and K -factors as defined in Eq. (52) (bottom) for third-generation slepton-pair and slepton-neutrino associated production at the LHC along the model line attached to the SPS 7 benchmark point (vertical dashed line). We show the total NLL+NLO matched and the fixed order NLO (SUSY-)QCD and LO QCD results.

$p \bar{p} \rightarrow \gamma, Z^0 \rightarrow \tilde{e}_L \tilde{e}_L^*$ at the Tevatron

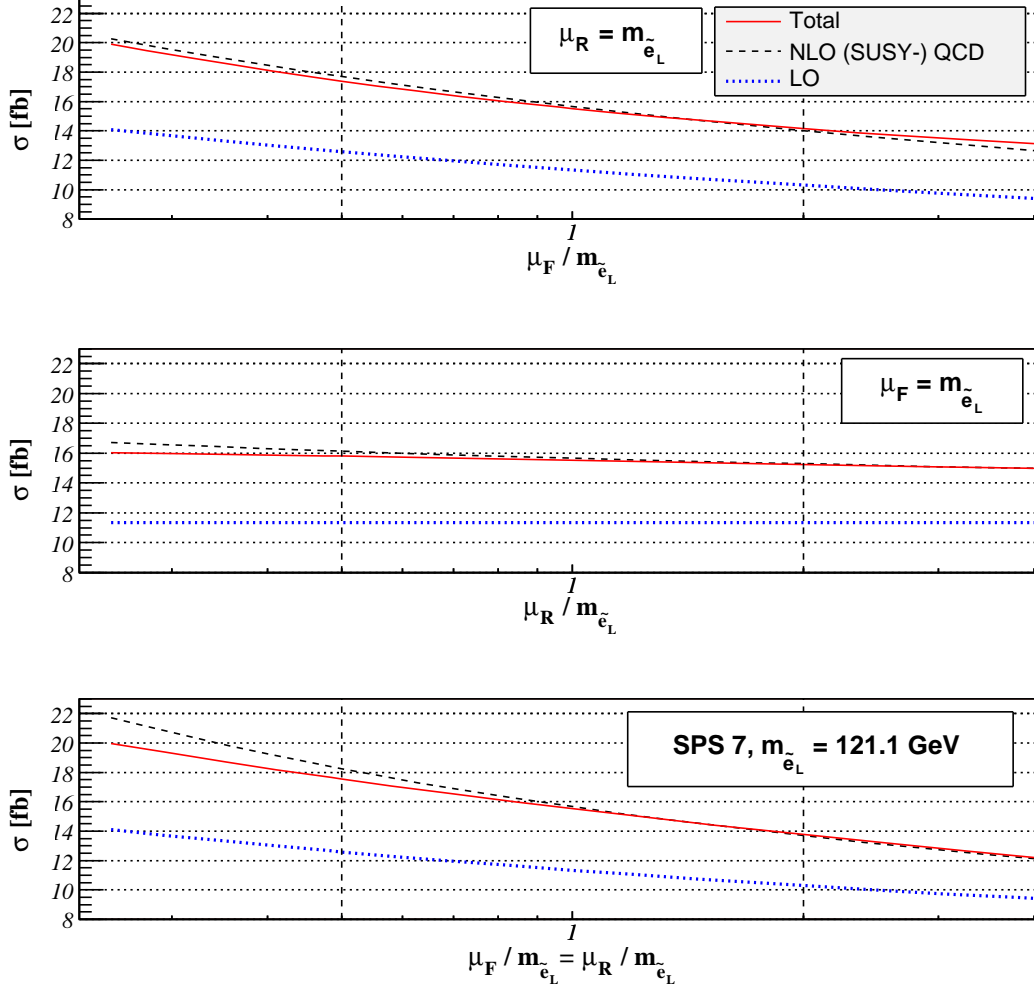


FIG. 10: Dependence of the total cross section for first- (and second-) generation slepton pairs at the Tevatron on the factorization scale (top), renormalization scale (middle), and both scales (bottom) for the SPS 7 benchmark point.

with

$$m_{LL}^2 = m_{\tilde{F}}^2 + (T_f^3 - e_f \sin^2 \theta_W) m_Z^2 \cos 2\beta, \quad (\text{A2})$$

$$m_{RR}^2 = m_{\tilde{F}'}^2 + e_f \sin^2 \theta_W m_Z^2 \cos 2\beta, \quad (\text{A3})$$

$$m_{LR} = A_f - \mu^* \begin{cases} \cot \beta & \text{for up-type sfermions.} \\ \tan \beta & \text{for down-type sfermions.} \end{cases} \quad (\text{A4})$$

It is diagonalized by a unitary matrix $S^{\tilde{f}}$, $S^{\tilde{f}} \mathcal{M}^2 S^{\tilde{f}\dagger} = \text{diag}(m_1^2, m_2^2)$, and has the squared mass eigenvalues

$$m_{1,2}^2 = m_f^2 + \frac{1}{2} \left(m_{LL}^2 + m_{RR}^2 \mp \sqrt{(m_{LL}^2 - m_{RR}^2)^2 + 4 m_f^2 |m_{LR}|^2} \right). \quad (\text{A5})$$

For real values of m_{LR} , the sfermion mixing angle $\theta_{\tilde{f}}$, $0 \leq \theta_{\tilde{f}} \leq \pi/2$, in

$$S^{\tilde{f}} = \begin{pmatrix} \cos \theta_{\tilde{f}} & \sin \theta_{\tilde{f}} \\ -\sin \theta_{\tilde{f}} & \cos \theta_{\tilde{f}} \end{pmatrix} \text{ with } \begin{pmatrix} \tilde{f}_1 \\ \tilde{f}_2 \end{pmatrix} = S^{\tilde{f}} \begin{pmatrix} \tilde{f}_L \\ \tilde{f}_R \end{pmatrix} \quad (\text{A6})$$

$pp \rightarrow \gamma, Z^0 \rightarrow \tilde{\tau}_1 \tilde{\tau}_1^*$ at the LHC

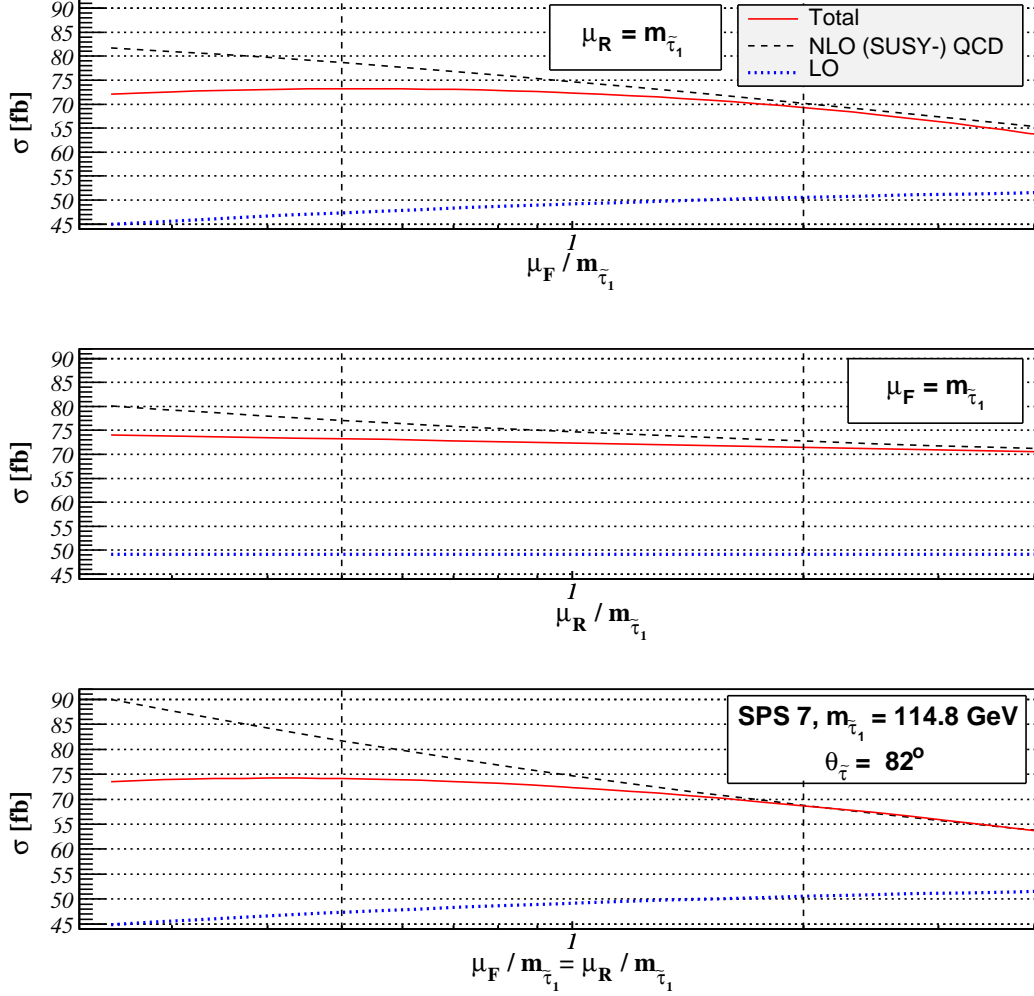


FIG. 11: Dependence of the total cross section for third-generation slepton pairs at the LHC on the factorization scale (top), renormalization scale (middle), and both scales (bottom) for the SPS 7 benchmark point.

can be obtained from

$$\tan 2\theta_{\tilde{f}} = \frac{2m_f m_{LR}}{m_{LL}^2 - m_{RR}^2}. \quad (\text{A7})$$

If m_{LR} is complex, one may first choose a suitable phase rotation $\tilde{f}'_R = e^{i\phi} \tilde{f}_R$ to make the mass matrix real and then diagonalize it for \tilde{f}'_L and \tilde{f}'_R . $\tan\beta = v_u/v_d$ is the (real) ratio of the vacuum expectation values of the two Higgs fields, which couple to the up-type and down-type (s)fermions. The soft SUSY-breaking mass terms for left- and right-handed sfermions are $m_{\tilde{F}}$ and $m_{\tilde{F}'}$, respectively.

APPENDIX B: SUSY-QCD FORM FACTORS FOR MIXED SQUARK MASS EIGENSTATES

At next-to-leading order in perturbative QCD, SUSY-QCD form factors are induced by one-loop diagrams involving gluinos and (generally mixed) squark mass eigenstates. Those appearing in the neutral-current cross section of Eq.

(17) are given by

$$f_\gamma = 2 + \sum_{i=1,2} \left[\frac{2m_g^2 - 2m_{\bar{q}_i}^2 + M^2}{M^2} \left(B_{0f}(M^2, m_{\bar{q}_i}^2, m_{\bar{q}_i}^2) - B_{0f}(0, m_g^2, m_{\bar{q}_i}^2) \right) + (m_{\bar{q}_i}^2 - m_g^2) B'_{0f}(0, m_g^2, m_{\bar{q}_i}^2) \right. \\ \left. + 2 \frac{m_g^4 + (M^2 - 2m_{\bar{q}_i}^2)m_g^2 + m_{\bar{q}_i}^4}{M^2} C_{0f}(0, M^2, 0, m_{\bar{q}_i}^2, m_g^2, m_{\bar{q}_i}^2) \right], \quad (\text{B1})$$

$$f_{\gamma Z} = 2(L_{Zqq} + R_{Zqq}) \\ + \sum_{i=1,2} \left[2 \frac{(2m_g^2 - 2m_{\bar{q}_i}^2 + M^2) \operatorname{Re} [L_{Z\bar{q}_i\bar{q}_i} + R_{Z\bar{q}_i\bar{q}_i}]}{M^2} B_{0f}(M^2, m_{\bar{q}_i}^2, m_{\bar{q}_i}^2) \right] \\ - \sum_{i=1,2} \left[2 \frac{(2m_g^2 - 2m_{\bar{q}_i}^2 + M^2) (L_{Zqq} |S_{i1}^{\bar{q}}|^2 + R_{Zqq} |S_{i1}^{\bar{q}}|^2)}{M^2} B_{0f}(0, m_g^2, m_{\bar{q}_i}^2) \right] \\ + \sum_{i=1,2} \left[(m_{\bar{q}_i}^2 - m_g^2) (L_{Zqq} + R_{Zqq}) B'_{0f}(0, m_g^2, m_{\bar{q}_i}^2) \right] \\ + \sum_{i=1,2} \left[4 \frac{(m_g^4 + (M^2 - 2m_{\bar{q}_i}^2)m_g^2 + m_{\bar{q}_i}^4) \operatorname{Re} [L_{Z\bar{q}_i\bar{q}_i} + R_{Z\bar{q}_i\bar{q}_i}]}{M^2} C_{0f}(0, M^2, 0, m_{\bar{q}_i}^2, m_g^2, m_{\bar{q}_i}^2) \right], \quad \text{and} \quad (\text{B2})$$

$$f_Z = 2(L_{Zqq}^2 + R_{Zqq}^2) \\ + \sum_{i,j=1,2} \left[2 \frac{(2m_g^2 - m_{\bar{q}_i}^2 - m_{\bar{q}_j}^2 + M^2)}{M^2} |L_{Z\bar{q}_i\bar{q}_j} + R_{Z\bar{q}_i\bar{q}_j}|^2 B_{0f}(M^2, m_{\bar{q}_i}^2, m_{\bar{q}_j}^2) \right] \\ - \sum_{i=1,2} \left[2 \frac{(2m_g^2 - 2m_{\bar{q}_i}^2 + M^2) (L_{Zqq}^2 |S_{i1}^{\bar{q}}|^2 + R_{Zqq}^2 |S_{i2}^{\bar{q}}|^2)}{M^2} B_{0f}(0, m_g^2, m_{\bar{q}_i}^2) \right] \\ + \sum_{i=1,2} \left[(m_{\bar{q}_i}^2 - m_g^2) (L_{Zqq}^2 + R_{Zqq}^2) B'_{0f}(0, m_g^2, m_{\bar{q}_i}^2) \right] \\ + \sum_{i,j=1,2} \left[4 \frac{(m_g^4 + (M^2 - m_{\bar{q}_i}^2 - m_{\bar{q}_j}^2)m_g^2 + m_{\bar{q}_i}^2 m_{\bar{q}_j}^2)}{M^2} |L_{Z\bar{q}_i\bar{q}_j} + R_{Z\bar{q}_i\bar{q}_j}|^2 C_{0f}(0, M^2, 0, m_{\bar{q}_i}^2, m_g^2, m_{\bar{q}_j}^2) \right], \quad (\text{B3})$$

and the one appearing in the charged-current cross section of Eq. (18) by

$$f_W = 2 |L_{Wqq'}|^2 \\ + \sum_{i,j=1,2} \left[\frac{2(2m_g^2 - m_{\bar{q}_i}^2 - m_{\bar{q}'_j}^2 + M^2)}{M^2} |L_{W\bar{q}_i\bar{q}'_j}|^2 B_{0f}(M^2, m_{\bar{q}_i}^2, m_{\bar{q}'_j}^2) \right] \\ - \sum_{\bar{Q}=\bar{q},\bar{q}'} \sum_{i=1,2} \left[\frac{(2m_g^2 - 2m_{\bar{Q}_i}^2 + M^2) B_{0f}(0, m_g^2, m_{\bar{Q}_i}^2) |L_{Wqq'} S_{i1}^{\bar{Q}}|^2}{M^2} \right] \\ + \sum_{\bar{Q}=\bar{q},\bar{q}'} \sum_{i=1,2} \left[\frac{1}{2} (m_{\bar{Q}_i}^2 - m_g^2) |L_{Wqq'}|^2 B'_{0f}(0, m_g^2, m_{\bar{Q}_i}^2) \right] \\ + \sum_{i,j=1,2} \left[\frac{4(m_g^4 - (m_{\bar{q}_i}^2 + m_{\bar{q}'_j}^2 - M^2)m_g^2 + m_{\bar{q}_i}^2 m_{\bar{q}'_j}^2)}{M^2} |L_{W\bar{q}_i\bar{q}'_j}|^2 C_{0f}(0, M^2, 0, m_{\bar{q}'_i}^2, m_g^2, m_{\bar{q}_j}^2) \right]. \quad (\text{B4})$$

The functions $B_{0f}(p^2, m_1^2, m_2^2)$, $B'_{0f}(p^2, m_1^2, m_2^2)$ and $C_{0f}(p_1^2, (p_1 + p_2)^2, p_2^2, m_1^2, m_2^2, m_3^2)$ are the finite parts of the scalar two- and three-point functions

$$B_0(p^2, m_1^2, m_2^2) = \mu_R^{2\epsilon} \int \frac{d^D q}{i\pi^2} \frac{1}{(q^2 - m_1^2)((q + p)^2 - m_2^2)}, \quad (\text{B5})$$

$$B'_0(p^2, m_1^2, m_2^2) = \left. \frac{dB_0(k^2, m_1^2, m_2^2)}{dk^2} \right|_{k^2=p^2}, \quad \text{and} \quad (\text{B6})$$

$$C_0(p_1^2, (p_1 + p_2)^2, p_2^2, m_1^2, m_2^2, m_3^2) = \mu_R^{2\epsilon} \int \frac{d^D q}{i\pi^2} \frac{1}{(q^2 - m_1^2)((q + p_1)^2 - m_2^2)((q + p_1 + p_2)^2 - m_3^2)}. \quad (\text{B7})$$

Our results agree with those of Ref. [45] in the case of mass-degenerate non-mixing squarks.

-
- [1] H.P. Nilles, Phys. Rept. **110** (1984) 1.
[2] H.E. Haber and G.L. Kane, Phys. Rept. **117** (1985) 75.
[3] E. Witten, Nucl. Phys. B **188** (1981) 513.
[4] S. Dimopoulos, S. Raby and F. Wilczek, Phys. Rev. D **24** (1981) 1681.
[5] J.R. Ellis, J.S. Hagelin, D.V. Nanopoulos, K.A. Olive and M. Srednicki, Nucl. Phys. B **238** (1984) 453.
[6] J.A. Aguilar-Saavedra *et al.*, Eur. Phys. J. C **46** (2006) 43.
[7] G. Bozzi, B. Fuks and M. Klasen, Phys. Rev. D **74** (2006) 015001.
[8] C.G. Lester and D.J. Summers, Phys. Lett. B **463** (1999) 99.
[9] A.J. Barr, JHEP **0602** (2006) 042.
[10] E. Lytken, Czech. J. Phys. **54** (2004) A169.
[11] Yu.M. Andreev, S.I. Bitjukov and N.V. Krasnikov, Phys. Atom. Nucl. **68** (2005) 340.
[12] W.M. Yao *et al.* [Particle Data Group], J. Phys. G **33** (2006) 1.
[13] S. Dawson, E. Eichten and C. Quigg, Phys. Rev. D **31** (1985) 1581.
[14] P. Chiappetta, J. Soffer and P. Taxil, Phys. Lett. B **162** (1985) 192.
[15] F. del Aguila and L. Ametller, Phys. Lett. B **261** (1991) 326.
[16] H. Baer, C.H. Chen, F. Paige and X. Tata, Phys. Rev. D **49** (1994) 3283.
[17] G. Bozzi, B. Fuks and M. Klasen, Phys. Lett. B **609** (2005) 339.
[18] H. Baer, B.W. Harris and M.H. Reno, Phys. Rev. D **57** (1998) 5871.
[19] W. Beenakker, M. Klasen, M. Krämer, T. Plehn, M. Spira and P.M. Zerwas, Phys. Rev. Lett. **83** (1999) 3780.
[20] G. Sterman, Nucl. Phys. B **281** (1987) 310.
[21] S. Catani and L. Trentadue, Nucl. Phys. B **327** (1989) 323 and *ibid.* **353** (1991) 183.
[22] A. Vogt, Phys. Lett. B **497** (2001) 221.
[23] S. Catani, D. de Florian, M. Grazzini and P. Nason, JHEP **0307** (2003) 028.
[24] S. Moch, J.A.M. Vermaseren and A. Vogt, Nucl. Phys. B **726** (2005) 317.
[25] S. Moch and A. Vogt, Phys. Lett. B **631** (2005) 48.
[26] E. Laenen and L. Magnea, Phys. Lett. B **632** (2006) 270.
[27] A. Bartl, K. Hidaka, K. Hohenwarter-Sodek, T. Kernreiter, W. Majerotto and W. Porod, Eur. Phys. J. C **46** (2006) 783.
[28] S. Catani and M.H. Seymour, Nucl. Phys. B **485** (1997) 291 [Erratum-*ibid.* B **510** (1998) 503].
[29] W. Furmanski and R. Petronzio, Z. Phys. C **11** (1982) 293.
[30] G. Altarelli and G. Parisi, Nucl. Phys. B **126** (1977) 298.
[31] G.P. Korchemsky, Mod. Phys. Lett. A **4** (1989) 1257.
[32] J. Kodaira and L. Trentadue, Phys. Lett. B **112** (1982) 66; Phys. Lett. B **123** (1983) 335.
[33] S. Catani, E. D’Emilio and L. Trentadue, Phys. Lett. B **211** (1988) 335.
[34] S. Catani, M.L. Mangano, P. Nason and L. Trentadue, Nucl. Phys. B **478** (1996) 273.
[35] M. Krämer, E. Laenen and M. Spira, Nucl. Phys. B **511** (1998) 523.
[36] S. Catani, D. de Florian and M. Grazzini, JHEP **0105** (2001) 025.
[37] T. O. Eynck, E. Laenen and L. Magnea, JHEP **0306** (2003) 057.
[38] O. Martin, A. Schäfer, M. Stratmann and W. Vogelsang, Phys. Rev. D **57** (1998) 3084.
[39] A. Djouadi, J.L. Kneur and G. Moultaka, hep-ph/0211331.
[40] B.C. Allanach *et al.*, Eur. Phys. J. C **25** (2002) 113.
[41] I. Hinchliffe, Nucl. Phys. Proc. Suppl. **123** (2003) 229.
[42] S. Gennai, Nucl. Phys. Proc. Suppl. **123** (2003) 244.
[43] A.D. Martin, R.G. Roberts, W.J. Stirling and R.S. Thorne, Phys. Lett. B **531** (2002) 216.
[44] A.D. Martin, R.G. Roberts, W.J. Stirling and R.S. Thorne, Phys. Lett. B **604** (2004) 61.
[45] A. Djouadi and M. Spira, Phys. Rev. D **62** (2000) 014004.
[46] While the top-squark mass eigenstate \tilde{t}_1 is slightly lighter, it does nonetheless not contribute to the virtual squark loops due to the negligible top-quark density in the proton.